

Circular motion of neutral test particles in Reissner-Nordström spacetime

Daniela Pugliese,^{*} Hernando Quevedo,[†] and Remo Ruffini[‡]

Dipartimento di Fisica, Università di Roma La Sapienza,

Piazzale Aldo Moro 5, I-00185 Roma, Italy

ICRANet, Piazzale della Repubblica 10, I-65122 Pescara, Italy.

(Dated: December 27, 2010)

Abstract

We investigate the motion of neutral test particles in the gravitational field of a mass M with charge Q described by the Reissner-Nordström (RN) spacetime. We focus on the study of circular stable and unstable orbits around configurations describing either black holes or naked singularities. We show that at the classical radius, defined as Q^2/M , there exist orbits with zero angular momentum due to the presence of repulsive gravity. The analysis of the stability of circular orbits indicates that black holes are characterized by a continuous region of stability. In the case of naked singularities, the region of stability can split into two non-connected regions inside which test particles move along stable circular orbits.

PACS numbers: 04.20.-q, 04.40.Dg, 04.70.Bw

Keywords: Reissner-Nordström metric; naked singularity; black hole; test particle motion; circular orbits

^{*}Electronic address: daniela.pugliese@icra.it

[†]On sabbatical leave from Instituto de Ciencias Nucleares, Universidad Nacional Autónoma de México;

Electronic address: quevedo@nucleares.unam.mx

[‡]Electronic address: ruffini@icra.it

I. INTRODUCTION

In general relativity, the gravitational field of a static, spherically symmetric, charged body with mass M and charge Q is described by the Reissner-Nordström (RN) metric which in standard spherical coordinates can be expressed as

$$ds^2 = -\frac{\Delta}{r^2}dt^2 + \frac{r^2}{\Delta}dr^2 + r^2(d\theta^2 + \sin^2\theta d\phi^2) , \quad (1)$$

where $\Delta = r^2 - 2Mr + Q^2$, and the associated electromagnetic potential and field are

$$A = \frac{Q}{r}dt, \quad F = dA = -\frac{Q}{r^2}dt \wedge dr , \quad (2)$$

respectively. The horizons are situated at $r_{\pm} = M \pm \sqrt{M^2 - Q^2}$.

The study of the motion of test particles in this gravitational field is simplified by the fact that any plane through the center of the spherically symmetric gravitational source is a geodesic plane. Indeed, it can easily be seen that if the initial position and the tangent vector of a geodesic lie on a plane that contains the center of the body, then the entire geodesic must lie on this plane. Without loss of generality we may therefore restrict ourselves to the study of equatorial geodesics with $\theta = \pi/2$.

The tangent vector u^a to a curve $x^\alpha(\tau)$ is $u^\alpha = dx^\alpha/d\tau = \dot{x}^\alpha$, where τ is an affine parameter along the curve. The momentum $p^\alpha = \mu\dot{x}^\alpha$ of a particle with mass μ can be normalized so that $g_{\alpha\beta}\dot{x}^\alpha\dot{x}^\beta = -k$, where $k = 0, 1, -1$ for null, timelike, and spacelike curves, respectively. For the RN metric we obtain

$$-\frac{\Delta}{r^2}\dot{t}^2 + \frac{r^2}{\Delta}\dot{r}^2 + r^2\dot{\phi}^2 = -k \quad (3)$$

on the equatorial plane. The last equation reduces to a first-order differential equation

$$-\frac{E^2 r^2}{\mu^2 \Delta} + \frac{r^2}{\Delta}\dot{r}^2 + \frac{L^2}{\mu^2 r^2} = -k , \quad (4)$$

where we have used the expressions for the energy, $E \equiv -g_{\alpha\beta}\xi_t^\alpha p^\beta = \mu\frac{\Delta}{r^2}\dot{t}$, and angular momentum, $L \equiv g_{\alpha\beta}\xi_\phi^\alpha p^\beta = \mu r^2\dot{\phi}$ of the test particle which are constants of motion associated with the Killing vector fields $\xi_t = \partial_t$ and $\xi_\phi = \partial_\phi$, respectively. Equation (4) can be rewritten as

$$\dot{r}^2 + V^2 = \frac{E^2}{\mu^2} , \quad \text{with} \quad V \equiv \sqrt{\left(k + \frac{L^2}{\mu^2 r^2}\right) \left(1 - \frac{2M}{r} + \frac{Q^2}{r^2}\right)} . \quad (5)$$

The investigation of the motion of test particles in the gravitational field of the RN metric is thus reduced to the study of motion in the effective potential V . In this work, we will focus on the study of circular orbits for which $\dot{r} = 0$ and $V = E/\mu$, with the condition $\partial V/\partial r = 0$. A straightforward calculation shows that this condition leads to

$$\frac{L^2}{\mu^2} = k \frac{r^2(Mr - Q^2)}{r^2 - 3Mr + 2Q^2} , \quad (6)$$

an expression which we substitute in Eq. (5) to obtain (an alternative analysis using an orthonormal frame is presented in Appendix A)

$$\frac{E^2}{\mu^2} = k \frac{(r^2 - 2Mr + Q^2)^2}{r^2(r^2 - 3Mr + 2Q^2)} . \quad (7)$$

Moreover, from the physical viewpoint it is important to find the minimum radius for stable circular orbits which is determined by the inflection points of the effective potential function, i.e., by the condition $\partial^2 V/\partial^2 r = 0$. It is easy to show that for the potential (5), the last condition is equivalent to

$$Mr^3 - 6M^2r^2 + 9MQ^2r - 4Q^4 = 0 . \quad (8)$$

In this work, we present a detailed analysis of the circular motion of test particles governed by the above equations. We will see that the behavior of test particles strongly depends on the ratio Q/M and, therefore, we consider separately the case of black holes, extreme black holes and naked singularities.

II. BLACK HOLES

From the expressions for the energy and angular momentum of a timelike particle ($k = 1$) we see that motion is possible only for $r > Q^2/M = r_*$ and for $r^2 - 3Mr + 2Q^2 > 0$, i.e., $r < r_{\gamma_-}$ and $r > r_{\gamma_+}$, with $r_{\gamma_{\pm}} \equiv [3M \pm \sqrt{(9M^2 - 8Q^2)}]/2$. In fact, from Eqs.(6) and (7) it follows that the motion inside the regions $r < r_*$ and $r \in (r_{\gamma_-}, r_{\gamma_+})$ is possible only along spacelike geodesics. At $r = r_{\gamma_+}$ one finds instead that the velocity of test particles, as defined in Appendix A, is $\nu_{g_+} = 1$, i.e., the circle $r = r_{\gamma_+}$ represents a null hypersurface. On the other hand, for a non-vanishing charge in the black hole region one can show that

$$r_- < r_{\gamma_-} < r_* < r_+ < r_{\gamma_+}, \quad \text{with} \quad r_+ = r_- = r_{\gamma_-} = r_* \quad \text{for} \quad Q = M \quad (9)$$

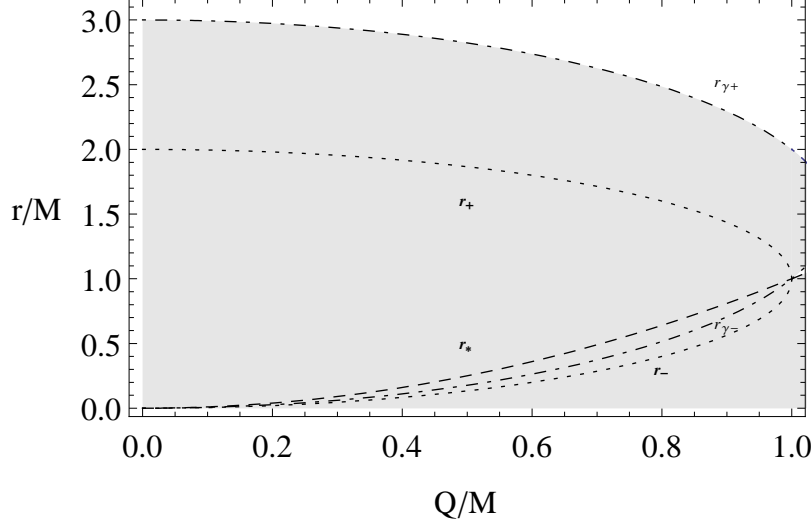


FIG. 1: In this graphic the radii $r_{\gamma+} \equiv [3M + \sqrt{(9M^2 - 8Q^2)}]/2$ and $r_{\pm} = M + \sqrt{M^2 - Q^2}$, and $r_* = Q^2/M$ are plotted. Timelike circular orbits exist only for $r > r_{\gamma+}$, whereas $r = r_{\gamma+}$ represents a null hypersurface. Circular motion inside the regions $r < r_*$ and $r \in (r_{\gamma-}, r_{\gamma+})$ is possible only along spacelike geodesics.

$$\text{and } r_- = r_{\gamma-} = r_* \quad \text{for } Q = 0 . \quad (10)$$

The location of these radii for different values of the mass-to-charge ratio is depicted in Fig. 1. In the black hole region we limit ourselves to the study of circular timelike orbits, i.e., orbits with $r > r_{\gamma+}$.

The effective potential (5) for a test particle with a fixed value of Q/M is plotted in Fig. 2, for different values of the angular momentum $L/(M\mu)$. At infinity, the effective potential tends to a constant which is independent of the value of the parameters of the test particle and of the gravitational source. In our case, this constant is normalized by choosing the value of the total energy of the particle as E/μ . Moreover, as the outer horizon is approached from outside, the effective potential reaches its global minimum value which is zero. This behavior is illustrated in Fig. 3 where the effective potential is depicted for a specific value of Q/M and different values of $L/(M\mu)$. The radius of a circular orbit, r_{co} , is determined by the real positive root of the equation

$$Mr^3 - \left(Q^2 + \frac{L^2}{\mu^2}\right)r^2 + \frac{3ML^2}{\mu^2}r - \frac{2Q^2L^2}{\mu^2} = 0 . \quad (11)$$

In general, in the region $r > r_{\gamma+}$ circular orbits do not always exist. For instance, for $Q = 0$ circular orbits exist only for values of $|L/(\mu M)| > \sqrt{12} \approx 3.45$, whereas for $Q = M$ and

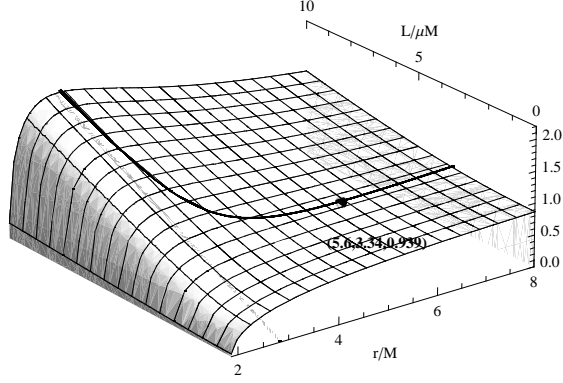


FIG. 2: The effective potential V for a neutral particle of mass μ in a RN black hole of charge-to-mass ratio $Q/M = 0.5$, is plotted as function of r/M in the range $[1.87, 8]$, and the angular momentum L/μ in $[0, 10]$. In this case the outer horizon $r_+ = 1.87M$, and $r_{\gamma_+} = 2.823M$ (see text). Circular orbits exist for $r > 2.823M$. The solid line represents the location of circular orbits (stable and unstable). The last circular orbit is represented by a point. The number close to the plotted point represent the radius $r/M = 5.6$, the angular momentum $L/\mu = 3.34$ and the energy $E/M = 0.939$ of the last stable circular orbit.

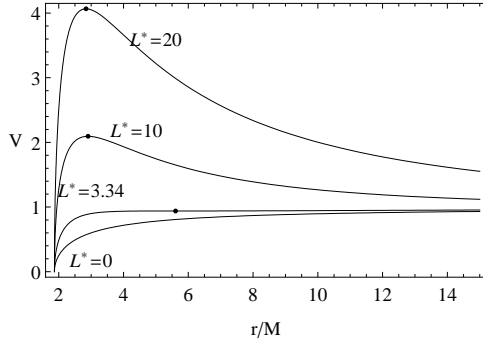


FIG. 3: The effective potential V for a neutral particle of mass μ in a RN black hole of charge Q and mass M is plotted in terms of the radius r/M for different values of the angular momentum $L^* \equiv L/(M\mu)$ and $Q = 0.5M$. The outer horizon is located at $r_+ \approx 1.87M$. The effective potential has a minimum, $V_{min} \approx 0.93$, at $r_{min} \approx 5.60M$, for $L^* \approx 3.34$. The plotted points represent local extrema.

$Q = 0.5M$ the existence condition implies that $|L/(\mu M)| > \sqrt{8} \approx 2.83$ and $|L/(\mu M)| > 3.33$, respectively.

In this context, it is interesting to explore the stability properties of the circular motion at $r = r_{co}$. To find the explicit value of the last stable radius we solve the condition (8) in

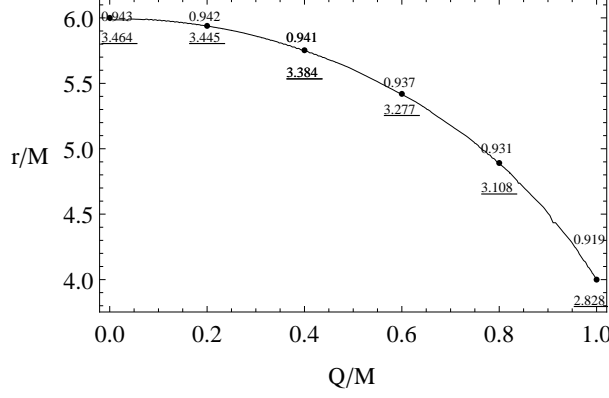


FIG. 4: The radius of the last stable orbit r_{LSCO}/M is plotted as a function of the ratio Q/M . Numbers close to the points represent the value of the energy E/μ and of the angular momentum $L/(\mu M)$ (underlined numbers) of the corresponding orbit.

the black hole region and find

$$\frac{r_{\text{LSCO}}}{M} = 2 + \frac{4 - \frac{3Q^2}{M^2} + \left[8 + \frac{2Q^4}{M^4} + \frac{Q^2 \left(-9 + \sqrt{5 - \frac{9Q^2}{M^2} + \frac{4Q^4}{M^4}} \right)}{M^2} \right]^{2/3}}{\left[8 + \frac{2Q^4}{M^4} + \frac{Q^2 \left(-9 + \sqrt{5 - \frac{9Q^2}{M^2} + \frac{4Q^4}{M^4}} \right)}{M^2} \right]^{1/3}}. \quad (12)$$

As expected, in the limiting case $Q \rightarrow 0$, we obtain the Schwarzschild value $r_{\text{LSCO}}^{\text{max}} = 6M$. The value of r_{LSCO} decreases as Q/M increases, until it reaches its minimum value $r_{\text{LSCO}}^{\text{min}} = 4M$ at $Q/M = 1$. The general behavior of r_{LSCO} in terms of the ratio Q/M is illustrated in Fig. 4.

Orbits with $r > r_{\text{LSCO}}$ are stable. Circular motion in the region $r_{\gamma_+} < r < r_{\text{LSCO}}$ is completely unstable. Since the velocity of a test particle at $r = r_{\gamma_+}$ must equal the velocity of light, one can expect that a particle in the unstable region will reach very rapidly the orbit at $r = r_{\text{LSCO}}$. For a static observer inside the unstable region, the hypersurface $r = r_{\gamma_+}$ might appear as a source of “repulsive gravity”. This intuitive result can be corroborated by analyzing the behavior of energy and angular momentum of test particles. Indeed, Figs. 5 shows E/μ and $L/(M\mu)$ as functions of r/M , for different values of the charge-to-mass ratio of the black hole. Both quantities diverge as the limiting radius $r = r_{\gamma_+}$ is approached, indicating that an infinite amount of energy and angular momentum is necessary to reach $r = r_{\gamma_+}$. As the ratio Q/M increases, the values of the energy and angular momentum at the last stable orbit decrease. For large values of the radius, the energy of circular orbits

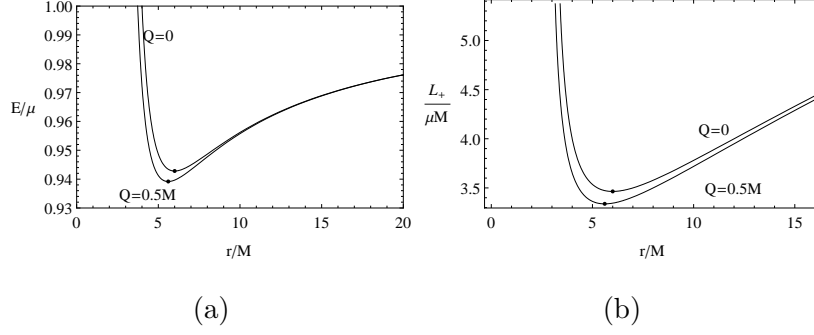


FIG. 5: The pictures show (a) the energy E/μ and (b) the angular momentum $L_+/(M\mu) \equiv L^*$ of a circular orbit as a function of r/M . Notice that for $Q = 0$, the relevant radii are $r_+ = 2M$ and $r_{\gamma_+} = 3M$, and the minima are $E_{min}/\mu \approx 0.943$ and $L_{min}^* \approx 3.46$, with $r_{min} = 6M$. Furthermore, for $Q = 0.5M$, we obtain $r_+ \approx 1.87M$ and $r_{\gamma_+} \approx 2.83M$, so that the minima are $E_{min}/\mu \approx 0.939$ and $L_{min}^* \approx 3.34$, with $r_{min} \cong 5.61M$. The energy and angular momentum diverge as the limiting radius r_{γ_+} is approached.

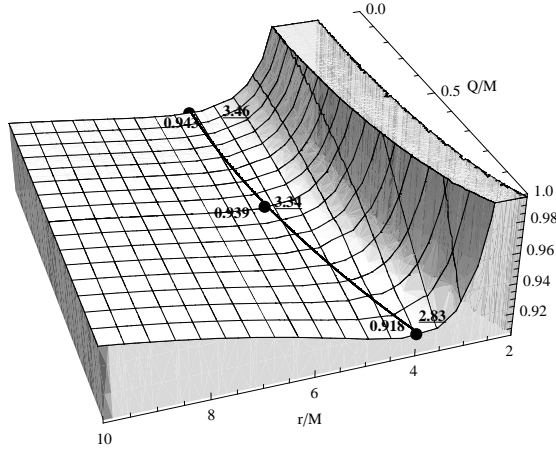


FIG. 6: The energy E/μ of a test particle on a circular orbit as a function of r/M and charge-to-mass ratio $Q/M \in [0, 1]$. The radius of the last stable circular orbit is also plotted (thick line). Numbers close to the points correspond to the energy and the angular momentum (underlined numbers) of the last stable circular orbit.

approaches the limit $E = \mu$, and the angular momentum $L/(M\mu)$ increases monotonically. A more detailed illustration of this behavior in the case of the energy of the test particle is represented in Fig. 6 which shows E/μ in terms of the ratio Q/M and the radial distance r/M .

The analytical expressions for the energy and angular momentum at the last stable orbit

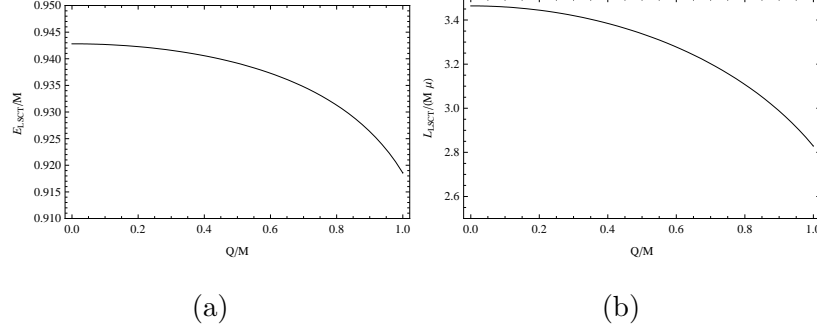


FIG. 7: Plots of the energy E_{LSCO}/M (a), and the angular momentum $L_{\text{LSCO}}/(\mu M)$ (b) of the last stable circular orbit in terms of the ratio Q/M of the black hole.

can be obtained by introducing the expression (12) into Eqs. (6) and (7). A numerically analysis of the resulting expressions show the behavior depicted in Fig. (7).

As a general result we obtain that the values for the radius of the last stable orbit as well as of the corresponding energy and angular momentum diminish due to the presence of the electric charge. Physically, this means that the additional gravitational field generated by the electric charge acts on neutral particles as an additional attractive force which reduces the radius of the last stable orbit.

A. Extreme black hole

In the case of an extreme black hole ($Q = M$) the outer and inner horizons coincide at $r_{\pm} = M$. The effective potential vanishes at the horizon and tends to 1 as spatial infinity is approached. In this open interval no divergencies are observed. This behavior is illustrated in Fig. 8 where the effective potential

$$V = \sqrt{1 + \frac{L^2}{\mu^2 r^2}} \left(1 - \frac{M}{r}\right) \quad (13)$$

is plotted for different values of the angular momentum $L/(M\mu)$. For $Q = M$ the radius of circular orbits is

$$\frac{r_{\text{CO}}}{M} = \frac{L^2 - L\sqrt{-8\mu^2 M^2 + L^2}}{2\mu^2 M^2}. \quad (14)$$

The energy and angular momentum of test particles moving along circular orbits are given by

$$\frac{E^2}{\mu^2} = \frac{(r - M)^3}{r^2(r - 2M)}, \quad \frac{L^2}{\mu^2} = \frac{Mr^2}{r - 2M}. \quad (15)$$

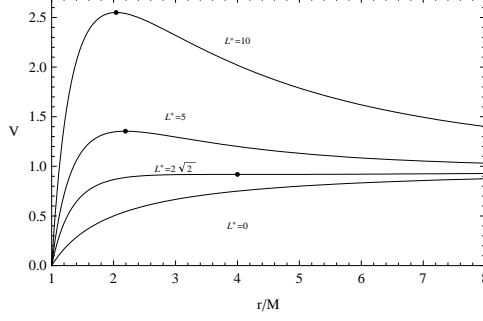


FIG. 8: The effective potential V for a neutral particle of mass μ in the field of an extreme RN black hole is plotted as function of the radius r/M for different values of the angular momentum $L^* \equiv L/(M\mu)$. The outer horizon is located at $r_+ = M$. For $L^* \approx 2.83$ the effective potential has a minimum $V_{min} \approx 0.91$ at $r_{min} = 4M$. There is a maximum $V_{max} \approx 1.35$ at $r \approx 2.19M$ for $L^* = 5$, and for $L^* = 10$ the maximum $V_{max} \approx 2.55$ is located at $r \approx 2.04M$.

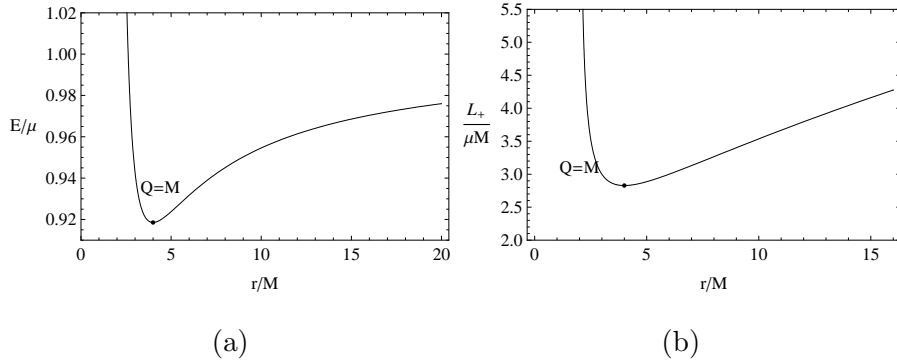


FIG. 9: Plots of (a) the energy E/μ and (b) the angular momentum $L_+/(M\mu) \equiv L^*$ of a neutral test particle in circular motion around an extreme RN black hole. The outer horizon is $r_+ = M$ and $r_{\gamma_+} = 2M$. At $r = 4M$ the minimum values of the energy $E_{min}/\mu \approx 0.91$ and angular momentum $L_{min}^* \approx 2.83$ are reached.

Consequently, timelike circular orbits are restricted by the condition $r > r_{g+} = 2M$. Figure 9 shows the behavior of these quantities in terms of the radial distance. As $r \rightarrow 2M$, the energy and angular momentum diverge, indicating that the circular motion at r_{γ_+} is possible only along null geodesics. As expected, the local minimum of these graphics determine the radius of the last stable orbit. At $r = r_{\text{LSO}} = 4M$, the energy is $E \approx 0.918\mu$ and the angular momentum $L = 2\sqrt{2}\mu M$.

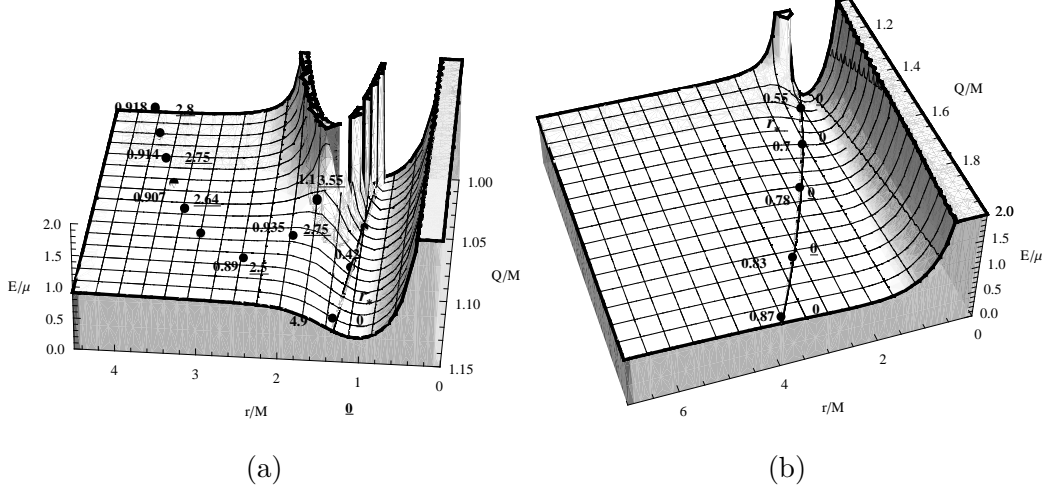


FIG. 10: Plot of the energy E/μ of a neutral particle in circular motion around a RN naked singularity as a function of r/M and Q/M in the interval $[1, 1.6]$ (a) and in the interval $[1.1, 2]$ (b). The line $r_* = Q^2/M$ is also plotted. Numbers close to the points represent the energy and the angular momentum (underlined numbers) of the last stable circular orbits.

III. NAKED SINGULARITY

In the naked singularity case $Q > M$ and the energy and angular momentum of the test particle can be written as

$$\frac{E}{\mu} = \frac{r^2 - 2Mr + Q^2}{r\sqrt{r^2 - 3Mr + 2Q^2}}, \quad \frac{L_+}{\mu} = +r\sqrt{\frac{Mr - Q^2}{r^2 - 3Mr + 2Q^2}}. \quad (16)$$

In Fig. 10 a three-dimensional plot shows the energy as a function of both the circular orbits radius and the charge-to-mass ratio of the black hole.

From the expressions for energy and angular momentum we see that it is necessary to consider four different cases: the value $r = r_* = Q^2/M$, the region inside the interval $1 < Q^2/M^2 < 9/8$, the value $Q^2/M^2 = 9/8$, and finally the region defined by $Q^2/M^2 > 9/8$. In Figs. 11-12 the behavior of the effective potential is exemplified for different values of the ratio Q/M .

Notice that for a RN naked singularity ($Q/M > 1$) the following inequality holds

$$r_* \leq r_{\gamma_-} \leq r_{\gamma_+}, \quad (17)$$

where $r_{\gamma_{\pm}} \equiv [3M \pm \sqrt{(9M^2 - 8Q^2)}]/2$ are the radii at which the value of the angular momentum and the energy of the test particle diverge.

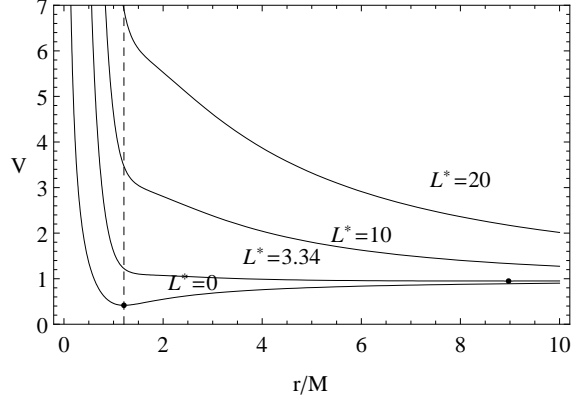


FIG. 11: The effective potential V for a neutral particle of mass μ in a RN naked singularity with $Q/M = 1.1$ is plotted as a function of the radius r/M for different values of the angular momentum $L^* \equiv L/(M\mu)$. The classical radius $r_* \equiv Q^2/M = 1.21M$ is represented by a dashed line. For $L^* = 0$ the effective potential presents a minimum $V_{min} \approx 0.42$ at $r_{min} = r_*$. For $L^* \approx 3.37$ the minimum $V_{min}/\mu \approx 0.95$ is situated at $r_{min} \approx 8.97M$.

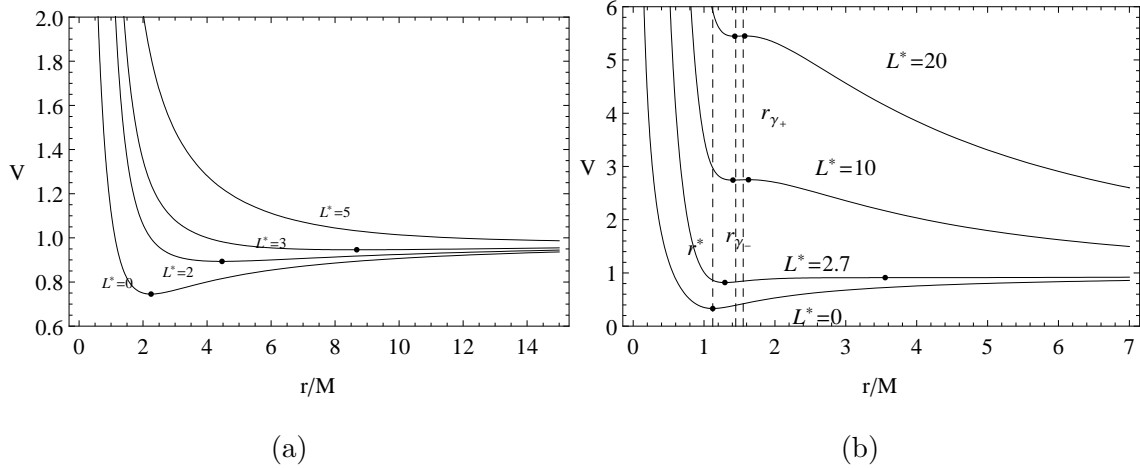


FIG. 12: The effective potential V for a neutral particle of mass μ in a RN naked singularity. Plot (a) is for $Q/M = 1.5$ so that $r_* = Q^2/M = 2.25M$. For the lowest value $L^* = 0$ at $r = r_*$ there is global minimum with $V_{min} \approx 0.74$. The value of V_{min} increases as L^* increases. Plot (b) corresponds to $Q/M = 1.06$, and shows the characteristic radii $r_* = 1.12M$, $r_{\gamma+} \equiv [3M + \sqrt{(9M^2 - 8Q^2)}]/2 \approx 5.55M$ and $r_{\gamma-} \equiv [3M - \sqrt{(9M^2 - 8Q^2)}]/2 \approx 1.44M$. For $L^* = 0$ the global minimum is at $r = r_*$ with $V_{min} \approx 0.33$. As L^* increases, the value of V_{min} increases, and at $L^* \approx 2.7$ a second local minimum appears. The first one with $V_{min} \approx 0.81$ is at $r_{min} \approx 1.29M$ and the second one with $V_{min} \approx 0.91$ is located at $r_{min} \approx 3.5M$.

A. Static test particles

Consider the orbit at $r = r_*$. In the naked singularity case the time-like condition for the velocity ν_g is satisfied only for $r \geq r_*$ (see Eq. (A4)). In the limiting case $r = r_*$, a time-like orbit with

$$L(r_*) = 0, \quad \frac{E}{\mu} = \sqrt{1 - \frac{M^2}{Q^2}} \quad (18)$$

is allowed. It is interesting to note that $r_* = Q^2/M$ coincides with the value of the classical radius of an electric charge which is usually obtained by using a completely different approach. This value appears here as the radius at which a particle can remain “static” with respect to an observer at infinity. This is an interesting situation which can be explained intuitively only by assuming the existence of a “repulsive” force. The above expression for the energy of the particle indicates that only in the case of a naked singularity a real value for the energy can be obtained. In fact, in the case of a black hole, the radius r_* is situated inside the outer horizon so that r_* cannot be reached by classical test particles. We conclude that the “repulsive” force can be the dominant gravitational force only in the case of a naked singularity.

B. The interval $1 < Q^2/M^2 < 9/8$

In the first region, for $1 < Q^2/M^2 < 9/8$ (see Fig. 12b), time-like circular orbits can exist in the regions $r_* < r < r_{\gamma-}$ and $r > r_{\gamma+}$. The boundaries $r = r_{\gamma\pm}$ correspond to null geodesics, as can be seen from the expression for the velocity along circular orbits as defined in Appendix A ($\nu_{g\pm} = 1$). This implies that there are two regions defined by $r < r_*$ and $r \in [r_{\gamma-}, r_{\gamma+}]$ where no time-like particles can be found. This behavior is schematically illustrated in Fig. 13. In the limiting case $Q^2/M^2 \rightarrow 1$, the classical radius coincides with $r_{\gamma-}$ and therefore the only particle that can remain “static” on the classical radius must be a photon.

C. The case $Q^2/M^2 = 9/8$

For $Q^2/M^2 = 9/8$, the exterior and interior photon orbits situated at $r_{\gamma+}$ and $r_{\gamma-}$ coincide. The effective potential behaves as illustrated in Fig. 14. Local minima can be found in

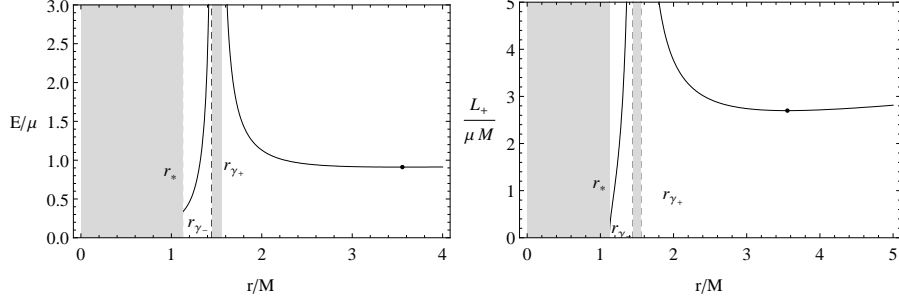


FIG. 13: The pictures show (a) the energy E/μ and (b) the angular momentum $L_+/(M\mu) \equiv L^*$ of a neutral particle moving on circular orbit around a RN naked singularity with $Q/M = 1.06 < \sqrt{9/8}$. The shaded regions are forbidden, i.e., circular orbits can exist only in the regions defined by $r_* < r < r_{\gamma-}$ and $r > r_{\gamma+}$, where $r_* = Q^2/M \approx 1.12M$, $r_{\gamma-} \equiv [3M - \sqrt{(9M^2 - 8Q^2)}]/2 \approx 1.44M$, and $r_{\gamma+} \equiv [3M + \sqrt{(9M^2 - 8Q^2)}]/2 \approx 1.55M$ (see text). A minimum for the energy and the angular momentum is located at $r_{min} \approx 3.55M$, where $L_{min}^* \approx 2.69$ and $E_{min}/\mu \approx 0.91$. Moreover, $L^*(r_*) = 0$ and $(E_{min}/\mu)(r_*) \approx 0.33$.

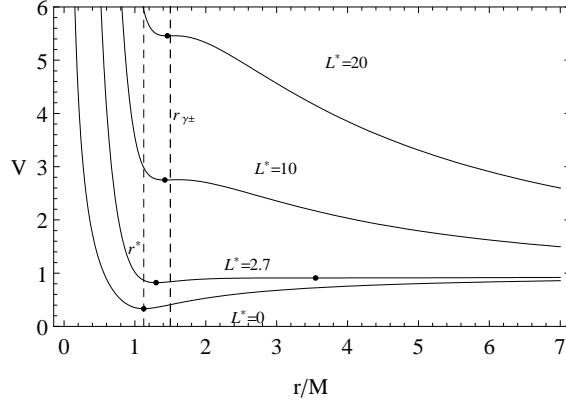


FIG. 14: The effective potential V for a neutral particle of mass μ in a RN naked singularity with $Q/M = \sqrt{9/8}$ is plotted as function of the radius r/M for different values of the angular momentum $L^* \equiv L/(M\mu)$. In this case, $r_* = Q^2/M = 1.12M$ and $r_{\gamma\pm} \equiv [3M \pm \sqrt{(9M^2 - 8Q^2)}]/2 = 1.5M$.

different regions, depending on the value of the angular momentum of the test particle. Time-like circular orbits exists for all $r > r_*$, except at $r = r_{\gamma\pm} = 3M/2$, which corresponds to a photon orbit. The energy and angular momentum of circular orbits are given by

$$\frac{E}{\mu} = \frac{r^2 - 2Mr + \frac{9}{8}M^2}{r(r - \frac{3}{2}M)}, \quad \frac{L_+}{\mu} = +r \frac{\sqrt{M(r - \frac{9}{8}M)}}{r - \frac{3}{2}M}, \quad (19)$$

and are plotted in Fig. 15. As the photon orbits are approached, the particle velocity tends to $\nu_g = 1$ and the energy and angular momentum diverge.

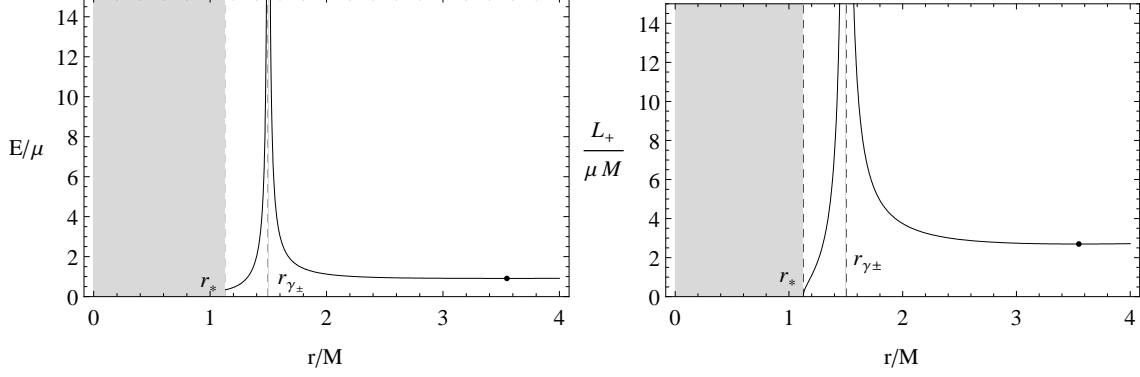


FIG. 15: Behavior of (a) the energy E/μ and (b) the angular momentum $L_+/(M\mu) \equiv L^*$ of a neutral particle moving along a circular orbit around a RN naked singularity with $Q/M = \sqrt{9/8}$. Shaded regions are forbidden for time-like particles.

D. The region $Q^2/M^2 > 9/8$

For $Q^2/M^2 > 9/8$, the effective potential behaves as illustrated in Figs. 11 and 12a. Time-like circular orbits can exist for all $r > r_*$. The time-like velocity condition ($\nu_g < 1$) is always satisfied so that no limiting photon orbits can exist in this case. The energy and the angular momentum are plotted in Figs. 16 and 17. The angular momentum increases as the radius of the orbit r/M increases. In the limit of large values of r , the energy tends to $E = \mu$.

E. The last stable circular orbit

To analyze the stability of circular orbits around a RN naked singularity we solve Eq. (8) under the assumption that $Q > M$. It turns out that real solutions exist only in the interval $1 < Q/M < \sqrt{5}/2$. They can be represented as

$$r_{lsc}^- = 2M + 2\sqrt{4M^2 - 3Q^2} \cos \left[\frac{1}{3} \arccos \left(\frac{8M^4 - 9M^2Q^2 + 2Q^4}{M(4M^2 - 3Q^2)^{3/2}} \right) \right], \quad (20)$$

$$r_{lsc}^+ = 2M - 2\sqrt{4M^2 - 3Q^2} \sin \left[\frac{1}{3} \arcsin \left(\frac{8M^4 - 9M^2Q^2 + 2Q^4}{M(4M^2 - 3Q^2)^{3/2}} \right) \right], \quad (21)$$

and

$$r_c = 2M - 2\sqrt{4M^2 - 3Q^2} \sin \left[\frac{\pi}{6} + \frac{1}{3} \arccos \left(\frac{8M^4 - 9M^2Q^2 + 2Q^4}{M(4M^2 - 3Q^2)^{3/2}} \right) \right]. \quad (22)$$

However, it can be shown that in this interval it holds that $r_c < Q^2/M = r_*$, i. e., this solution is located inside the classical radius where no time-like circular geodesics are allowed.

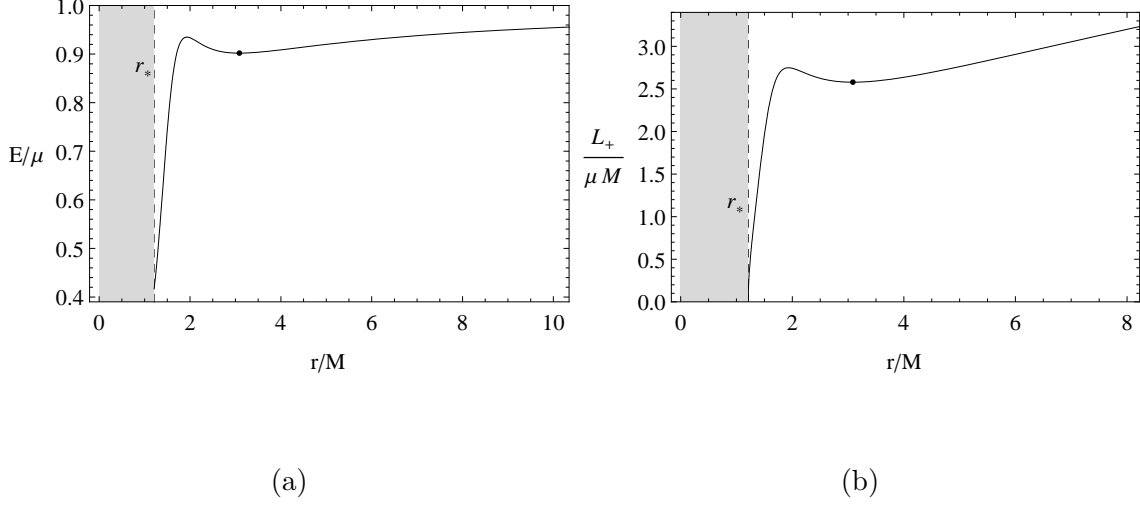


FIG. 16: The pictures show (a) the energy E/μ and (b) the angular momentum $L_+/(M\mu) \equiv L^*$ of a neutral particle moving along a circular orbit in a RN naked singularity with $Q/M = 1.1$ as a function of r/M . The shaded regions are forbidden. Circular orbits can exist only for $r > r_* \approx 1.21M$. A minimum of the energy and the angular momentum is located at $r_{min} \approx 3.08M$, where $L^*_{min} \approx 2.57$ and $E_{min}/\mu \approx 0.90$. Moreover, $L^*(r_*) = 0$ and $(E_{min}/\mu)(r_*) \approx 0.33$.

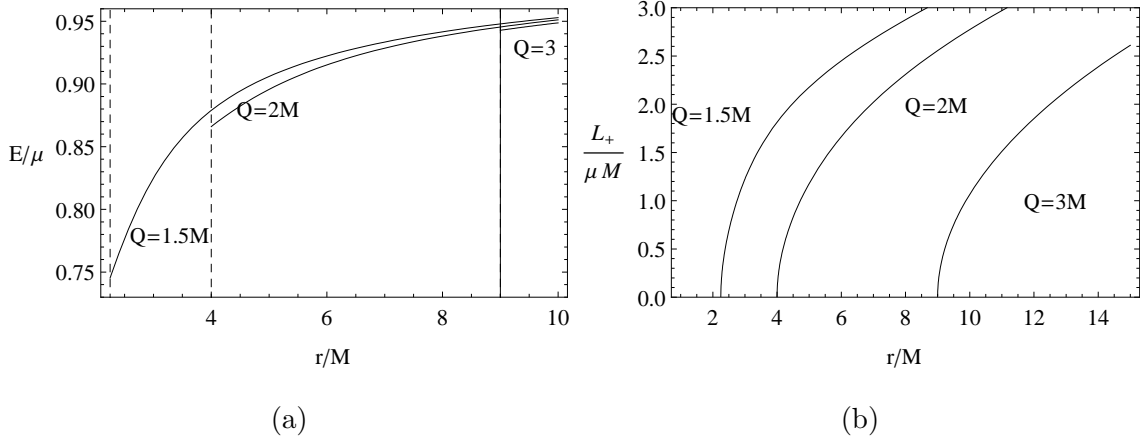


FIG. 17: The pictures show (a) the energy E/μ and (b) the angular momentum $L_+/(M\mu)$ of a test particle of mass μ in the field of a RN naked singularity as a function of r/M and for different values of the ratio Q/M , satisfying the condition $(Q/M)^2 > 9/8$ (see text). Circular orbits can exist only for $r > r_* \equiv Q^2/M$.

Moreover, $r_{lSCO}^- < r_{lSCO}^+$ in the entire interval, except at $Q/M = \sqrt{5}/2$ where $r_{lSCO}^- = r_{lSCO}^+$. For $Q/M > \sqrt{5}/2$ no solutions of Eq. (8) exist in the region defined by $r > Q^2/M$ so that for $(Q/M)^2 > 9/8$ the last stable “circular” orbit is located precisely at $r = r_* = Q^2/M$. This situation is sketched in Fig. 18 where it can be seen that the energy of a particle located at

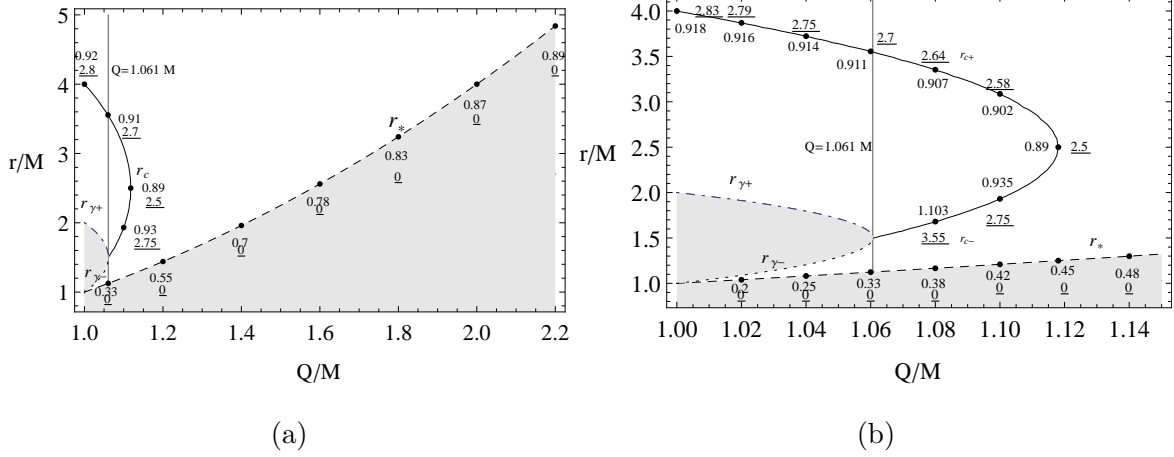


FIG. 18: The radius of the last stable circular orbit (solid line) of a neutral particle moving in the field of a RN naked singularity. The ratio Q/M varies in the interval $[1, 2.2]$ in plot (a), and in the interval $[1, 1.15]$ in plot (b). The dashed curve represents the classical radius $r_* = Q^2/M$. The dotted curve corresponds to photon orbits with radius $r_{\gamma-} = [3M - \sqrt{(9M^2 - 8Q^2)}]/2$, whereas the dot-dashed curve denotes the photon orbits with radius $r_{\gamma+} = [3M + \sqrt{(9M^2 - 8Q^2)}]/2$. Shaded regions are forbidden. In the interval $1 < Q/M < 1.061$ circular orbits can exist only for $r_* < r < r_{\gamma-}$ (all stable) and $r > r_{\gamma+}$ (unstable for $r_{\gamma+} < r < r_{lsc}^+$ and stable for $r > r_{lsc}^+$). For $Q/M > 1.061$ and $r > r_*$ the region of stability divides into two separated regions: $r_* < r < r_{lsc}^-$ and $r > r_{lsc}^+$. The numbers close to the plotted points denote the energy E/μ and the angular momentum $L/(\mu M)$ (underlined numbers) of the last stable circular orbits.

$r = r_*$ increases as the charge-to-mass ratio increases. In the interval $1 < Q/M < \sqrt{5}/2$, the energy and angular momentum of circular orbits situated on $r = r_{lsc}^+$ increase as the ratio Q/M increases. On the contrary, in the interval $\sqrt{9/8} < Q/M < \sqrt{5}/2$, the energy and angular momentum of circular orbits with radius $r = r_{lsc}^-$ increase as the ratio Q/M decreases. This is due to the fact that at $Q/M = \sqrt{9/8}$, the radius r_{lsc}^- coincides with the radii $r_{\gamma+}$ and $r_{\gamma-}$ which correspond to photon-like orbits. For $Q/M > \sqrt{5}/2$, the last stable circular orbit is situated at the classical radius $r_* = Q^2/M$ and the entire region $r > r_*$ is a region of stability. For $\sqrt{9/8} < Q/M < \sqrt{5}/2$, there are two regions of stable orbits, namely, $r_* < r < r_{lsc}^-$ and $r > r_{lsc}^+$, separated by a zone of instability defined by $r_{lsc}^- < r < r_{lsc}^+$. For $1 < Q/M < \sqrt{9/8}$, two regions of stable orbits appear at $r_* < r < r_{\gamma-}$ and at $r > r_{lsc}^+$; these regions are separated by the forbidden region, $r_{\gamma-} < r < r_{\gamma+}$, in which no circular time-like orbits exist, and by the instability region located at $r_{\gamma+} < r < r_{lsc}^+$.

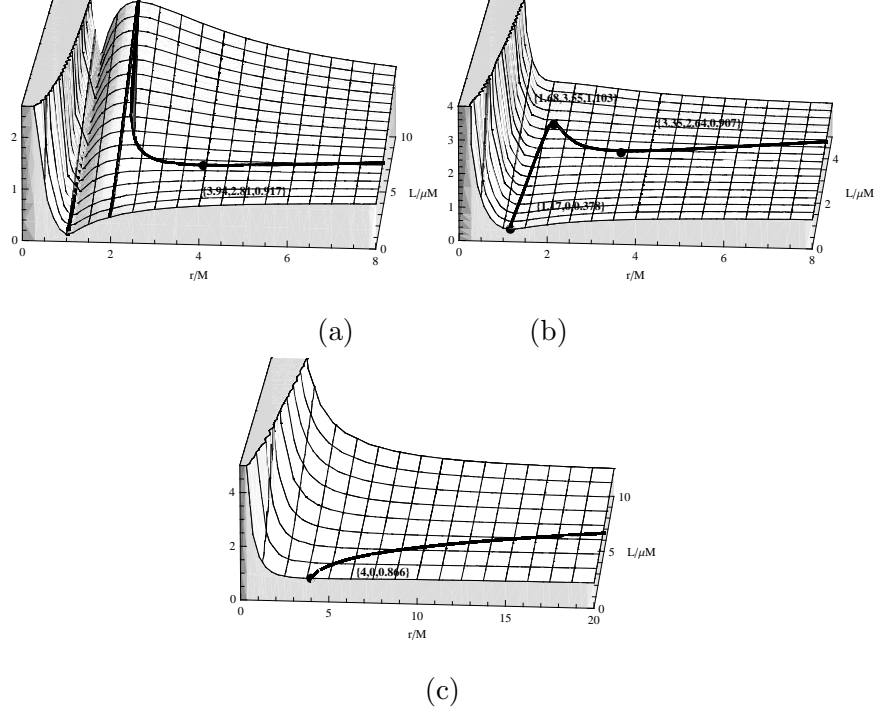


FIG. 19: The effective potential V for a neutral particle of mass μ in a RN naked singularity is plotted as a function of the radius r/M and of the angular momentum $L^* \equiv L/(M\mu)$. Solid lines represent the radii of circular orbits. The last stable circular orbit radius is denoted by a point. Plot (a) is for $Q = 1.1M$ so that $r_{\gamma-} = 1.04M$, $r_{\gamma+} = 1.95M$. The classical radius is $r_* \equiv Q^2/M = 1.21M$, where $L^* = 0$ and $V_{min} \approx 0.42$. Unstable circular orbits are in $r < 3.94M$ and at $r = 3.94M$, the values are $L^* \approx 2.81$ and $V/\mu \approx 0.91$. Plot (b) is for $Q = 1.08M$ so that $r_{\gamma\pm}$ do not exist and $r_* \equiv Q^2/M = 1.16M$ with $V_{min}(r_*) \approx 0.37$. Stable orbits are in the interval $r_* < r < 1.68M$ and at the boundary, $r = 1.68M$, the values are $L^* = 3.55$ and $V/\mu = 1.10$. The interval $1.68M < r < 3.35M$ corresponds to unstable orbits with the boundary values $L^* = 2.64$ and $V/\mu = 0.90$ at $r = 3.35M$. Stable orbits are located at $r > 3.35M$. Plot (c) is for $Q = 2M$ and $r_* = 4M$. Stable circular orbits exist for $r > 4M$ and at the boundary $V(4M) = 0.86\mu$.

The curves representing the radii of stable circular orbits are also showed in Fig. (19) where the effective potential is plotted for selected values of the Q/M as a function of the angular momentum and the radius.

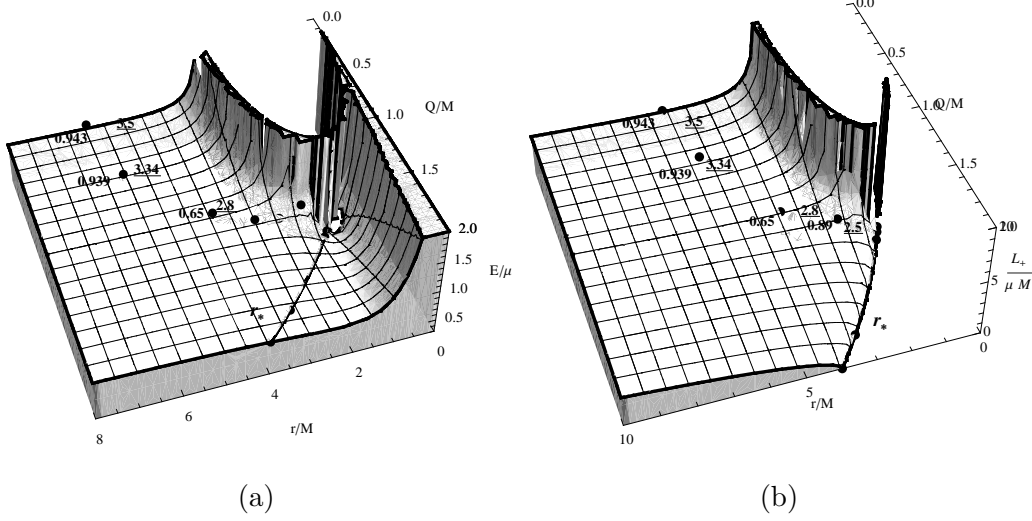


FIG. 20: The pictures show the energy E/μ (a) and the angular momentum $L_+ / (\mu M)$ (b) of a test particle moving along a circular orbit around a RN source as a function of r/M and the charge-to-mass ratio Q/M in the range $[0, 2]$. The curve $r = r_* \equiv Q^2/M$ is also plotted. The numbers close to the points denote the energy and the angular momentum (underlined numbers) of the last stable circular orbits.

IV. BLACK HOLE VERSUS NAKED SINGULARITY

The main results obtained from the study of RN black holes and naked singularities are here summarized and compared in the plots of Fig. 20–22.

In the three-dimensional plots of Fig. 20 the energy and the angular momentum (7) are shown as functions of the circular orbits radius and the charge-to-mass ratio Q/M , for both black hole and naked singularity cases.

Fig. 21 shows the circular orbits radius as a function of the angular momentum for different black holes and naked singularities. The cases of a Schwarzschild spacetime and the Newtonian limit are also plotted for comparison. Clearly, for large values of r/M all the curves converge to the Newtonian limit. Finally, the study of the circular orbits stability for neutral test particles in the RN spacetime is summarized in the Fig.22 where the radius of the last stable circular orbits is plotted as function of Q/M .

The location and structure of the stability regions for neutral particles around a black hole differ in a very strong way from the case of a naked singularity. Black hole sources are characterized by the existence of only one stability region which can extend from a

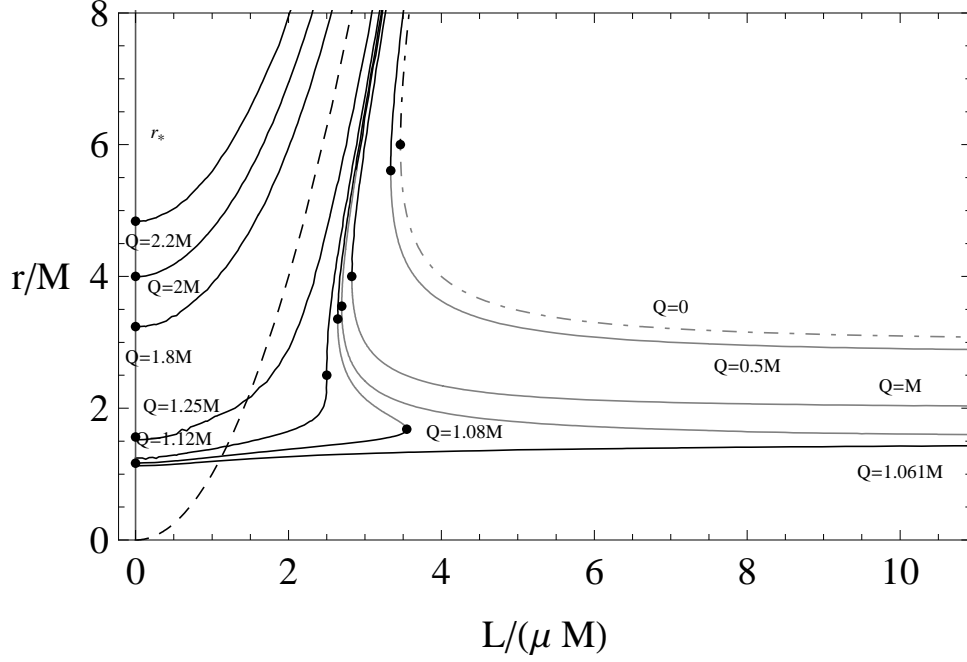


FIG. 21: The radius r/M of circular orbits for a neutral particle of mass μ in a RN geometry of charge Q and mass M is plotted as a function of the angular momentum $L/(\mu M)$ for different values of the charge-to-mass ratio Q/M in the interval $[0, 2]$. The radius of circular orbits for the Newtonian limit (dashed curve) and for the Schwarzschild spacetime (dot-dashed curve) are also plotted. The plotted points represent the last stable circular orbits. Black curves correspond to stable circular orbits, and gray curves denote unstable circular orbits. The dotted line represents the classical radius $r = r_* \equiv Q^2/M$.

minimum radius $r_{lsc} \in [4M, 6M]$ up to infinity. In the case of a naked singularity there are two possible scenarios. If the mass-to-charge ratio satisfies the condition $Q/M \geq \sqrt{5}/2$, there exist only one stability region which extends from the classical radius $r_* = Q^2/M$ up to infinity. The second scenario appears in naked singularities with charge-to-mass ratio within the range $1 < Q/M < \sqrt{5}/2$. In this case, we have two stability regions separated by either a region of instability or a forbidden region, where no time-like circular orbits are allowed, and a region of instability.

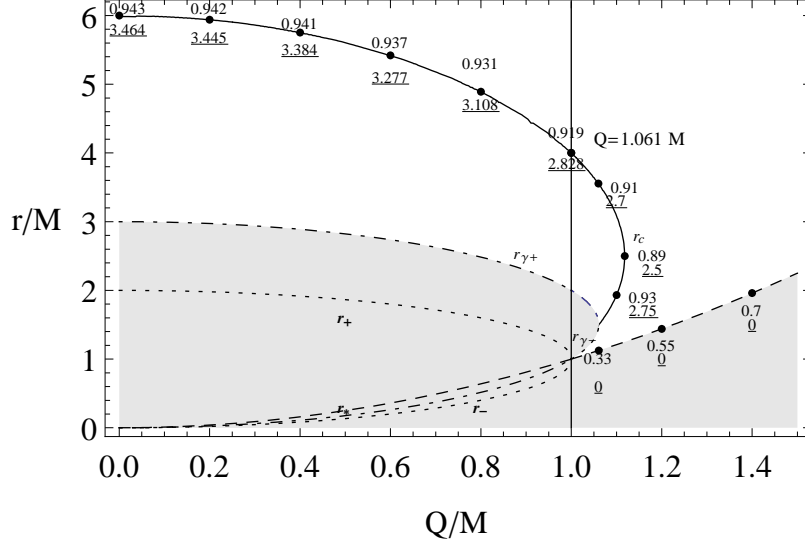


FIG. 22: The radius r/M of the last stable circular orbit of a neutral particle of mass μ in a RN geometry of charge Q and mass M is plotted as a function of the ratio Q/M in the interval $[0, 1.5]$. Here $r_{\gamma\pm} \equiv [3M \pm \sqrt{(9M^2 - 8Q^2)}]/2$ and $r_{\pm} \equiv M \pm \sqrt{M^2 - Q^2}$ (see text). In the Schwarzschild case, $Q = 0$, we find $r_{lSCO} = 6M$, $r_+ = 2M$ and $r_{\gamma+} = 3M$. For an extreme black hole, $Q = M$, we find $r_{lSCO} = 4M$ with $r_+ = M$ and $r_{\gamma+} = 2M$. The numbers close to the plotted points denote the energy E/μ and the angular momentum $L/(\mu M)$ (underlined numbers) of the last stable circular orbit.

V. CONCLUSIONS

In this work we discussed the motion of neutral test particles along circular orbits in the RN spacetime. We studied separately the case of black holes and naked singularities, emphasizing their differences. Our analysis is based on the study of the behavior of an effective potential that determines the position and stability properties of circular orbits. We also investigated in detail the behavior of the energy and angular momentum of the test particle in all possible configurations of black holes and naked singularities.

We found that at the classical radius $r = r_* = Q^2/M$ circular orbits exist with “zero” angular momentum. This means that a static observer situated at infinity would interpret this situation as a test particle that remains motionless ($r = Q^2/M = \text{const}$, $\phi = \text{const}$) as time passes. This phenomena can take place only in the case of a naked singularity and is interpreted as a consequence of the “repulsive” force generated by the charge distribution.

Black holes turn out to be characterized by a single zone of stability which extends from

a minimum radius r_{lsc} up to infinity. The radius of the last stable circular orbit has its maximum value of $r_{lsc} = 6M$ in the Schwarzschild limiting case, and reaches its minimum value of $r_{lsc} = 4M$ in the case of an extreme black hole. The situation is completely different in the case of naked singularities. If the mass-to-charge ratio satisfies the condition $Q/M \geq \sqrt{5}/2$, there exist only one stability region which extends from the classical radius $r_* = Q^2/M$ up to infinity. In this case, the classical radius determines also the radius of the last stable orbit that could be, in principle, as large as allowed by the amount of charge Q that can be associated to a given mass M . If the charge-to-mass ratio is within the range $1 < Q/M < \sqrt{5}/2$, we found two stability regions that are separated either by a region of instability, in the interval $\sqrt{9/8} < Q/M < \sqrt{5}/2$, or a region of instability and a region forbidden for time-like orbits, in the interval $1 < Q/M < \sqrt{9/8}$. This result implies that around a naked singularity with $1 < Q/M < \sqrt{5}/2$ the region of stability splits into two non-connected regions in which test particles can remain orbiting forever.

Acknowledgments

We would like to thank A. Geralico for helpful comments. Two of us (DP and HQ) thank ICRA-Net support. This work was supported in part by DGAPA-UNAM, grant No. IN106110.

Appendix A

Let us introduce an orthonormal frame adapted to the static observers:

$$e_{\hat{t}} = r\Delta^{-1/2}\partial_t, \quad e_{\hat{r}} = \frac{\Delta^{1/2}}{r}\partial_r, \quad e_{\hat{\theta}} = \frac{1}{r}\partial_\theta, \quad e_{\hat{\phi}} = \frac{1}{r\sin\theta}\partial_\phi \quad (\text{A1})$$

with dual

$$\omega^{\hat{t}} = \frac{\Delta^{1/2}}{r}dt, \quad \omega^{\hat{r}} = r\Delta^{-1/2}dr, \quad \omega^{\hat{\theta}} = r d\theta, \quad \omega^{\hat{\phi}} = r\sin\theta d\phi \quad (\text{A2})$$

Consider the tangent to a (time-like) spatially circular orbit u^a as

$$u = \Gamma(\partial_t + \zeta\partial_\phi) = \gamma[e_{\hat{t}} + \nu e_{\hat{\phi}}],$$

where Γ and γ are two normalization factors:

$$\Gamma^2 = (-g_{tt} - \zeta^2 g_{\phi\phi})^{-1} \quad \text{and} \quad \gamma^2 = (1 - \nu^2)^{-1}$$

which assures that $u_a u^a = -1$; where ζ is the angular velocity with respect to infinity and ν is the “local proper linear velocity” as measured in the frame (A1). The angular velocity ζ is related to the local proper linear velocity by

$$\zeta = \sqrt{-\frac{g_{tt}}{g_{\phi\phi}}} \nu.$$

so that $\Gamma = \gamma/\sqrt{-g_{tt}}$. Here ζ and therefore also ν are assumed to be constant along the u -orbit. As usually we limit our analysis to the equatorial plane; as a convention, the physical (orthonormal) component along $-\partial_\theta$, perpendicular to the equatorial plane will be referred to as along the positive z -axis and will be indicated by \hat{z} and so $e_{\hat{z}} = -e_{\hat{\theta}}$. Here we focus attention to the time-like circular geodesic u_\pm such that $\nabla_{u_\pm} u_\pm = 0$, co-rotating (ζ_+) and counter-rotating (ζ_-) with respect to the assumed positive (counter-clockwise) variation of the ϕ -angle respectively. It results:

$$\zeta_\pm \equiv \pm \zeta_g = \pm \frac{\sqrt{(Mr - Q^2)}}{r^2} \quad (\text{A3})$$

so that

$$\nu_g = \sqrt{\frac{Mr - Q^2}{\Delta}}, \quad \gamma_g = \left(\frac{\Delta}{r^2 - 3Mr + 2Q^2} \right)^{1/2} \quad (\text{A4})$$

$$u_\pm = \frac{\gamma_g}{\sqrt{-g_{tt}}} (\partial_t \pm \zeta_g \partial_\phi) = \gamma_g [e_{\hat{t}} \pm \nu_g e_{\hat{\phi}}], \quad (\text{A5})$$

with time-like condition $\nu_g < 1$ satisfied.

The particle's four-momentum is given by $p^a = \mu u^a$ where u^a is given by (A5). The conserved quantities associated with temporal and azimuthal Killing vectors ξ_t and ξ_ϕ are respectively

$$p_\alpha \xi_t^\alpha = -\mu \sqrt{-g_{tt}} \gamma_g = -E; \quad p_\alpha \xi_\phi^\alpha = \pm \mu \frac{\gamma_g \zeta_g r^2}{\sqrt{-g_{tt}}} = L_\pm$$

where E and L are the particle's energy and angular momentum respectively. Substituting the (A4) we infer:

$$\frac{E}{\mu} = \frac{\Delta}{r \sqrt{r^2 - 3Mr + 2Q^2}}, \quad \frac{L_\pm}{M\mu} = \pm \frac{r \sqrt{r - \frac{Q^2}{M}}}{\sqrt{M} \sqrt{r^2 - 3Mr + 2Q^2}} \quad (\text{A6})$$

these results are in agreement with the results obtained by the study of the effective potential.

-
- [1] R. Ruffini *On the Energetics of Black Holes, Le Astres Occlus*, (Le Houche 1972).
- [2] C. W. Misner, K. S. Thorne, and J. A. Wheeler, *Gravitation* (Freeman, San Francisco, 1973).
- [3] S. Chandrasekhar, *The Mathematical Theory of Black Holes* (Oxford University Press, New York, 1983).
- [4] J. M. Cohen and R. Gautreau, Phys. Rev. D **19**, 2273 (1979).
- [5] P. Pradhan and P. Majumdar, arXiv:1001.0359 [gr-qc].
- [6] V. D. Gladush and M. V. Galadgyi, arXiv:1011.0843 [gr-qc].
- [7] A. N. Aliev, Class. Quant. Grav. **10** (1993) 1741.
- [8] W. B. Bonnor, Phys. Lett. A **83**, 414 (1981).
- [9] E. P. T. Liang, Phys. Rev. D **9** (1974) 3257.
- [10] Z. Stuchlik and S. Hledik, Acta Phys. Slov. **52** (2002) 363.
- [11] V. D. Gladush and M. V. Galadgyi, Kinematics and Physics of Celestial Bodies, 2009, Vol. 25, No. 2, pp. 7988.
- [12] N. Dadhich, J. Math. Phys. **20**, 1555 (1979).
- [13] J. Bičák, Z. Stuchlík, and V. Balek, *Bull. Astron. Inst. Czech.* **40**, 65-92 (1989).